Scalar Fields, Black Holes and Spherical Coordinates

Gonçalo Andrade*
CENTRA, Departamento de Física, Instituto Superior Técnico, Universidade de Lisboa
Avenida Rovisco Pais 1, 1049 Lisboa, Portugal
(Dated: January 13, 2021)

Black holes are some of the simplest objects predicted by General Relativity, yet they give rise to a number of interesting phenomena in their vicinities. Amongst these is the interaction of matter fields with the geometry, through quasi-normal oscillations and gravitational wave emission. Studying such phenomena could provide valuable insights towards dark matter searches from gravitational wave astronomy and other sources of astrophysical data.

In this thesis we explore the scattering of real scalar fields, described by the Klein-Gordon equation, with black hole spacetimes. Our approach focuses on the use of spherical coordinates to take advantage of the approximate symmetries of the problem. To do so, we start by introducing the formalism of Numerical Relativity and the BSSN formulation, along with techniques that allow the use of general curvilinear coordinate systems. Then, we make use of those techniques to evolve both the metric quantities and matter variables in a non-linear fashion. We implemented, within the code generation tool NRPy+, modules that allow for the evolution of scalar fields minimally coupled to gravity. Our results for the non-linear scattering of massless fields, as well as the evolution of pseudo-bound states of massive fields, are consistent with previous linear and non-linear studies in the literature.

I. INTRODUCTION

General Relativity (GR) is currently the most widely accepted theory of gravitation. It was proposed by Einstein in 1915, and since then it has been able to explain several different phenomena, such as the bending of starlight by the sun [1] or the appearance of gravitational wave signals from binary black hole mergers [2]. Amongst its predictions are Black Holes (BH), regions of spacetime where the gravitational pull is so strong that nothing, not even light, can escape. BHs are very interesting objects because they are rather simple – they are described by the Kerr-Newman family of solutions [3], which depends only on the mass M, charge Q and spin per unit mass a – but they are responsible by exotic events, such as the aforementioned emission of gravitational waves. Therefore, they are extremely interesting to study, and quite important to move our understanding of the universe forward.

There are some problems for which GR does not provide an answer. One such problem is dark matter: according to GR predictions, the detectable matter present in galaxies is not enough to provide sufficient gravitational attraction to hold them together. Therefore, it is theorised that a form of matter that does not emit or reflect electromagnetic radiation is present, in large quantities, in most galaxies, and it is usually referred to as *dark matter*.

The literature lists several dark matter candidates that may help resolve this issue, and each of them may present different measurable signals one might detect from astrophysical sources. One such possibility is that of ultralight bosonic fields, of scalar or vector nature. This sort of matter can interact with rotating BHs and extract energy from them, in a phenomenon known as *superradiance* (see [4] for a review on the subject). It was demonstrated by Zel'dovich in 1972 [5] that a field of the form $\psi \propto e^{-i\omega t+im\varphi}$ is subject to superradiant amplification by an object with rotational velocity Ω if condition

$$\omega > m\Omega \tag{1}$$

is met. This is what happens in the vicinity of a Kerr BH if a scalar field with these characteristics is present. Furthermore, if the field is massive, an attractive potential is created and the field remains confined around the BH, whilst continuing to extract energy from it. This leads to exponential amplification of the scalar cloud, in a phenomenon that is commonly designated as a *superradiant instability* or *black hole bomb*.

This work aims to study some of the characteristic behaviours of scalar fields in BH spacetimes. To do so, we use Numerical Relativity (NR) techniques to perform non-linear evolutions of these systems. Furthermore, our approach is characterised by the use of spherical coordinates, which are better adapted to the problem at hand, but pose some additional difficulties.

This paper is structured as follows. In sec. II we introduce the basic concepts of numerical relativity, namely the 3+1 decomposition of the Einstein equations and the BSSN formulation. Then, in sec. III we address the challenges one is faced with when wanting to use NR techniques in curvilinear coordinate systems. In sec. IV we detail the implementation of initial data and evolution equations for the fields, in secs. V and VI we go over the results of our study, and in sec. VII we present our conclusions.

* goncalo.j.c.andrade@tecnico.ulisboa.pt

II. NUMERICAL RELATIVITY IN A NUTSHELL

NR is the study of Einstein's equations of GR using numerical techniques, and it emerged as a field of research almost at the same time that computers were created. Although numerical techniques for PDEs are well-known, solving Einstein's equations on a computer requires major theoretical work. There are several approaches to this, but the most used one – and the one onto which we focus our attention – is the 3+1 Formalism. It is based on a Hamiltonian formulation of GR by Arnowitt, Deser and Misner [6] and, in simple terms, it amounts to decomposing spacetime into 3-dimensional space which evolves along a time coordinate t. For complete references on the subject, we recommend the books [7–9].

The split between time and space is done by introducing a *foliation* consisting of a family of spacelike 3-dimensional hypersurfaces $\{\Sigma_t\}, t \in \mathbb{R}$, each corresponding to a level surface of the scalar field t, which acts as a global time coordinate. Defining a future-directed unit normal vector to Σ_t, n^a, the metric induced on each sheet of the foliation by the spacetime metric g_{ab} is

$$\gamma_{ab} = g_{ab} + n_a n_b. \tag{2}$$

We describe the embedding of Σ_t into spacetime through the extrinsic curvature, defined as

$$K_{ab} = -\frac{1}{2}\mathcal{L}_n \gamma_{ab}, \tag{3}$$

where $\mathcal{L}_n$ is the Lie derivative along n^a. It is also useful to define two quantities, the lapse function α and the shift vector β^a. The lapse tells us how much proper time elapses, for a Eulerian observer, when going from a hypersurface Σ_t to another $\Sigma_{t+\mathrm{d}t}$, while the shift is related to the change of the local coordinates when moving from one slice to the next.

Taking the 4-dimensional Riemman tensor and performing multiple contractions with n^a and projections onto Σ_t gives the Gauss-Codazzi equations. Manipulating them, with the aid of the Einstein equations, yields evolution equations for γ_{ij}, K_{ij} (henceforth we use spatial indices, $i, j, ... = 1, 2, 3$, which can be shown to be the only relevant ones when dealing with spatial quantities) and two sets of constraints, referred to as the Hamiltonian and momentum constraints. These evolution equations are, however, only weakly hyperbolic, and are often unstable under numerical evolution.

The solution to this problem is the so called BSSN formulation, named after its creators [10, 11]. In this formulation, the spatial metric is conformally rescaled by a function ϕ, the conformal factor, through

$$\bar{\gamma}_{ij} = e^{-4\phi}\gamma_{ij}, \tag{4}$$

with $\bar{\gamma}_{ij}$ being the conformally related metric. The conformal factor is obtained by

$$\phi = \frac{1}{12}\ln\left(\frac{\gamma}{\eta}\right), \tag{5}$$

where $\gamma = \det\gamma_{ij}$ and $\eta = 1$ is the determinant of the flat metric in Cartesian coordinates. The extrinsic curvature is split into its trace K and a traceless part A_{ij},

$$K_{ij} = A_{ij} + \frac{1}{3}\gamma_{ij}K, \tag{6}$$

and the traceless part is conformally rescaled in the same way as the spatial metric. Furthermore, we introduce the conformal connection functions,

$$\bar{\Gamma}^i = \bar{\gamma}^{jk}\bar{\Gamma}^i_{jk} = -\partial_j\bar{\gamma}^{ij}, \tag{7}$$

which, if evolved alongside the rest of the metric quantities, renders the system strongly hyperbolic. Manipulation of the 3+1 evolution equations, along with these new definitions, gives the BSSN evolution equations,

$$\partial_t\phi = -\frac{1}{6}\alpha K + \beta^i\partial_i\phi + \frac{1}{6}\partial_i\beta^i, \tag{8a}$$

$$\partial_t\bar{\gamma}_{ij} = -2\alpha\bar{A}_{ij} + \beta^k\partial_k\bar{\gamma}_{ij} + \bar{\gamma}_{ik}\partial_j\beta^k + \bar{\gamma}_{kj}\partial_i\beta^k - \frac{2}{3}\bar{\gamma}_{ij}\partial_k\beta^k, \tag{8b}$$

$$\begin{aligned}\partial_t K =& -\gamma^{ij}D_jD_i\alpha + \alpha\left(\bar{A}_{ij}\bar{A}^{ij} + \frac{1}{3}K^2\right)\\ &+ 4\pi\alpha\left(\rho + S\right) + \beta^i\partial_i K,\end{aligned} \tag{8c}$$

$$\begin{aligned}\partial_t\bar{A}_{ij} =& e^{-4\phi}\left[-\left(D_iD_j\alpha\right)^{\mathrm{TF}} + \alpha\left(R^{\mathrm{TF}}_{ij} - 8\pi S^{\mathrm{TF}}_{ij}\right)\right]\\ &+ \alpha\left(K\bar{A}_{ij} - 2\bar{A}_{il}\bar{A}^l_j\right) + \beta^k\partial_k\bar{A}_{ij}\\ &+ \bar{A}_{ik}\partial_j\beta^k + \bar{A}_{kj}\partial_i\beta^k - \frac{2}{3}\bar{A}_{ij}\partial_k\beta^k,\end{aligned} \tag{8d}$$

$$\begin{aligned}\partial_t\bar{\Gamma}^i =& -2\bar{A}^{ij}\partial_j\alpha + \beta^j\partial_j\bar{\Gamma}^i - \bar{\Gamma}^j\partial_j\beta^i + \frac{2}{3}\bar{\Gamma}^i\partial_j\beta_j\\ &+ 2\alpha\left(\bar{\Gamma}^i_{jk}\bar{A}^{kj} - \frac{2}{3}\bar{\gamma}^{ij}\partial_j K - 8\pi\bar{\gamma}^{ij}S_j + 6\bar{A}^{ij}\partial_j\phi\right)\\ &+ \frac{1}{3}\bar{\gamma}^{li}\partial_l\partial_j\beta^j + \bar{\gamma}^{lj}\partial_j\partial_l\beta^i,\end{aligned} \tag{8e}$$

where the superscript TF stands for the trace free part of that quantity. We also obtain the constraints

$$\begin{aligned}\mathcal{H} \equiv& -16\pi\rho + \frac{2}{3}K^2 - \bar{A}_{ij}\bar{A}^{ij}\\ &+ e^{-4\phi}\left(\bar{R} - 8\bar{\gamma}^{ij}\bar{D}_j\phi\bar{D}_i\phi - 8\bar{\gamma}^{ij}\bar{D}_j\bar{D}_i\phi\right) = 0,\end{aligned} \tag{8f}$$

$$\mathcal{M}^i \equiv e^{-4\phi}\left(\bar{D}_j\bar{A}^{ij} + 6\bar{A}^{ij}\bar{D}_j\phi - \frac{2}{3}\bar{\gamma}^{ij}\bar{D}_j K\right) = 0. \tag{8g}$$

The equations above include the source terms ρ, S, S_a and S_{ab}, which are given by the expressions

$$\rho = n_a n_b T^{ab}, \tag{9a}$$

$$S_a = -\gamma_a^b n^c T_{bc}, \tag{9b}$$

$$S_{ab} = \gamma_a^c \gamma_b^d T_{cd} \quad \text{and} \quad S = g^{ab} S_{ab}. \tag{9c}$$

The lapse α and the shift β^i are gauge quantities, and they represent, in NR, the intrinsic coordinate freedom of GR. However, the choice of gauge can make or break the stability of numerical evolutions. We postpone our choice until the next section.

III. BSSN IN CURVILINEAR COORDINATES

The derivation of the BSSN equations (8) above assumes Cartesian coordinates, namely when setting the determinant of the flat metric to unity. Although these coordinates are the most common in numerical evolutions, they are not the most natural choice for systems with exact or approximate symmetries. However, if the BSSN equations are to be written in other coordinate systems, one needs to consider the tensor density weights of each quantity, and the transformation rules can become quite cumbersome.

This difficulty was overcome by Brown [12], who introduced a covariant formulation of the BSSN equations. The approach is based on setting up a reference metric $\hat{\gamma}_{ij}$, usually taken as the flat metric in whichever coordinates one chooses, and decomposing the conformal spatial metric into a perturbation over $\hat{\gamma}_{ij}$,

$$\bar{\gamma}_{ij} = \hat{\gamma}_{ij} + \varepsilon_{ij}. \tag{10}$$

Furthermore, the conformal factor ϕ is now given by

$$\phi = \frac{1}{12} \ln \left(\frac{\gamma}{\bar{\gamma}} \right), \tag{11}$$

and instead of imposing $\bar{\gamma} = \eta$, we instead provide an evolution equation to $\bar{\gamma}$, using Brown's Lagrangian choice

$$\partial_t \bar{\gamma} = 0, \tag{12}$$

and provide the initial condition $\bar{\gamma}\,(t=0) = \hat{\gamma}$.

The issue of covariance is taken care of by noticing that Christoffel symbols do not transform as tensors, but differences between two sets of them do. With that in mind, we can define

$$\Delta^i_{jk} = \bar{\Gamma}^i_{jk} - \hat{\Gamma}^i_{jk}. \tag{13}$$

With this new quantity, we define a new evolution variable, analogous to the conformal connection functions of eq. (7), as

$$\bar{\Lambda}^i - \Delta^i = 0, \tag{14}$$

with Δ^i being obtained by contraction of Δ^i_{jk} with the inverse conformal metric $\bar{\gamma}^{ij}$. This allows us to re-write the evolution equations as

$$\left(\partial_t - \mathcal{L}_\beta\right) \varepsilon_{ij} = \frac{2}{3} \bar{\gamma}_{ij} \left(\alpha \bar{A}^k_k - \bar{D}_k \beta^k \right) + 2 \hat{D}_{(i} \beta_{j)} - 2\alpha \bar{A}_{ij}, \tag{15a}$$

$$\begin{aligned}\left(\partial_t - \mathcal{L}_\beta\right) \bar{A}_{ij} =& -\frac{2}{3} \bar{A}_{ij} \bar{D}_k \beta^k - 2\alpha \bar{A}_{ik} \bar{A}^k_j + \alpha \bar{A}_{ij} K \\ &+ e^{-4\phi} \left[-2\alpha \bar{D}_i \bar{D}_j \phi + 4\alpha \bar{D}_i \phi \bar{D}_j \phi + 4 \bar{D}_{(i} \alpha \bar{D}_{j)} \phi \right. \\ &\left. - \bar{D}_i \bar{D}_j \alpha + \alpha \bar{R}_{ij} \right]^{\mathrm{TF}},\end{aligned} \tag{15b}$$

$$\left(\partial_t - \mathcal{L}_\beta\right) \phi = \frac{1}{6} \left(\bar{D}_k \beta^k - \alpha K \right), \tag{15c}$$

$$\begin{aligned}\left(\partial_t - \mathcal{L}_\beta\right) K =& \frac{1}{3} \alpha K^2 + \alpha \bar{A}_{ij} \bar{A}^{ij} \\ &- e^{-4\phi} \left(\bar{D}^i \bar{D}_i \alpha + 2 \bar{D}^i \alpha \bar{D}_i \phi \right),\end{aligned} \tag{15d}$$

$$\begin{aligned}\left(\partial_t - \mathcal{L}_\beta\right) \bar{\Lambda}^i =& \bar{\gamma}^{jk} \hat{D}_j \hat{D}_k \beta^i + \frac{2}{3} \Delta^i \bar{D}_j \beta^j + \frac{1}{3} \bar{D}^i \bar{D}_j \beta^j \\ &- 2\bar{A}^{ij} \left(\partial_j \alpha - 6 \partial_j \phi \right) + 2 \bar{A}^{jk} \Delta^i_{jk} - \frac{4}{3} \alpha \bar{\gamma}^{ij} \partial_j K.\end{aligned} \tag{15e}$$

The constraint equations keep their form of eqs. (8f, 8g).

In regards to the gauge choice, we employ a covariant alternative to the standard gauge [13], as recommended by Brown [12]. This is done by imposing that α evolve according to the 1+log condition,

$$\partial_t \alpha = -2\alpha K, \tag{16}$$

while β^i evolves through a modified hyperbolic Gamma driver equation. This equation is second order in time, so we introduce an auxiliary variable B^i, defined as

$$\left(\partial_t - \beta^j \partial_j\right) \beta^i = B^i, \tag{17a}$$

thus making the system first order. The evolution of B^i is then given by

$$\left(\partial_t - \beta^j \partial_j\right) B^i = \frac{3}{4} \left(\partial_t - \beta^j \partial_j\right) \bar{\Lambda}^i - \eta B^i, \tag{17b}$$

where η here is a damping parameter and not the determinant of the flat metric.

The second problem with trying to evolve NR quantities in curvilinear coordinates, such as spherical polar coordinates, is that of coordinate singularities. It is easy to show that taking vector and tensor components from Cartesian to spherical coordinates results in expressions that diverge wherever $r \sin\theta = 0$. This behaviour is also evident in differential operators that feature in the evolution equations.

The solution for this issue is two-fold. Firstly, when setting up a numerical grid, one can avoid these singular points by, for example, setting up a cell-centred grid. An additional measure that can be taken is that of analytically eliminating these divergent dependences, as proposed in ref. [14]. This is done by writing tensor components in a non-coordinate basis, where the basis vectors are given by

$$\boldsymbol{e}_{(i)} = \frac{1}{F_i} \frac{\boldsymbol{\partial}}{\boldsymbol{\partial x^i}}, \tag{18}$$

where F_i are the orthogonal scale factors. These scale factors are defined, assuming an orthogonal coordinate system, by

$$F_i = \sqrt{\hat{\gamma}_{ii}}, \tag{19}$$

where there is no implied sum over the index i. The assumption of an orthogonal coordinate system garantees a diagonal reference metric. Computationally, writing tensor components in this way amounts to rescaling the usual components, in the coordinate system of choice, by multiplication of the adequate combination of scale factors. In the context of BSSN, we define new quantities h_{ij}, a_{ij}, λ^i, $\mathcal{V}^i$ and $\mathcal{B}^i$ as rescaled versions of ε_{ij}, $\bar{A}_{ij}$, $\bar{\Lambda}^i$, β^i and B^i, respectively, and rescale the evolution equations accordingly.

The third and final issue one needs to address in order to successfully evolve the BSSN quantities in curvilinear coordinates is that of inner boundaries. In Cartesian coordinates, the limits of the coordinate ranges correspond to physical outer boundaries of the system under study. However, in curvilinear coordinates, these may correspond to inner boundaries, due to the periodic nature of some coordinate functions (like the angular coordinates in spherical or cylindrical systems). This leads to the identification of grid points across inner boundaries with others in the interior of the domain, and necessitates the application of parity conditions to vector and tensor components.

The need for grid points across inner boundaries, computationally, stems from the fact that approximation of spatial derivatives, through methods such as finite differences, require the sampling of grid functions at a certain number of neighbouring points in each direction. Therefore, numerical implementations often resort to *ghost points*, which have coordinate values outside their defined ranges. Across inner boundaries, grid function values at the ghost points must be substituted by the corresponding values inside the domain, and this correspondence procedure requires that both the grid points corresponding to inner boundaries, as well as their inner images, be identified prior to evolution. This identification can be done, for example, by taking the coordinates of the ghost point, converting them to Cartesian and then back to the original coordinate system. If the original coordinates values match the converted ones, the point is at an outer boundary, otherwise it is at an inner boundary and the converted coordinates are those of the corresponding inner point.

When going across an inner boundary, the unit basis vectors in which we express vector and tensor quantities may flip their direction. Therefore, tensor components need to have parity conditions applied to them when a correspondence is made between a ghost point and the corresponding inner point. This can be done by computing the dot products between the unit basis vectors in the coordinates of the ghost point and the corresponding inner point,

$$P_i = \frac{\boldsymbol{\partial}}{\boldsymbol{\partial x^i}}\left(x^j_{\rm gp}\right) \cdot \frac{\boldsymbol{\partial}}{\boldsymbol{\partial x^i}}\left(x^j_{\rm new}\right) = \pm 1, \tag{20}$$

where $x^j_{\rm gp}$ and $x^j_{\rm new}$ are the original and converted coordinates of the ghost point, respectively. These parity values allow the correspondence of inner and ghost points to be made according to

$$T^{ijk...}_{lmn...}\left(x^a\right) = \left(\prod_\alpha P_\alpha\right) T^{ijk...}_{lmn...}\left(x^a_{\rm new}\right), \tag{21}$$

with $\alpha \in \{i, j, k, ..., l, m, n...\}$. Since, in BSSN, quantities are, at most, of rank 2, it is easy to establish, *a priori*, the set of all 10 parity conditions describing all possible parity types for scalars, vectors and rank-2 tensors.

IV. NUMERICAL IMPLEMENTATION

We now focus in our numerical implementation of the formalisms detailed above, as well as the coupling of scalar fields to the evolution of the geometric quantities. Our implementation is based on NRPy+ [14], a Python-based tool that aims to generate highly optimised C code for NR. The base code of NRPy+ was augmented by several modules that add the ability for the evolution of scalar fields in curved geometries.

A. Overview of NRPy+

Before the details of the new modules are revealed, let us quickly review some features of NRPy+. In broad terms, NRPy+ has the ability to define symbolic expressions for evolution equations and initial data, through its use of the Python library *SymPy*. Then, using common subexpression elimination, it outputs C code that implements these expressions, as well as means to evolve them in time, using OpenMP parallelisation [15] and SIMD vectorisation.

NRPy+ implements a *Method of Lines* (MoL) evolution scheme, where the grid functions are sampled in a discrete spatial grid and are evolved through time using a time-stepping algorithm, such as a Runge-Kutta method. The grid is, as discussed above, set up to be cell-centred, meaning that singular points are avoided, and one can choose from a number of coordinate systems, such as Cartesian, spherical, cylindrical and rescalings of these. A particularly important coordinate system for the scope of this work is the *SinhSpherical* one, in which the radial coordinate r is given by

$$r = R_{\rm max}\frac{\sinh\left(\frac{\mathtt{x0}}{w_s}\right)}{\sinh\left(\frac{1}{w_s}\right)} \tag{22}$$

in terms of the NRPy+'s internal radial coordinate `x0`, which takes values in between 0 and 1 in this case. This rescaling of r allows for a higher sampling of the spacetime near the origin, whilst pushing the boundary away to reduce the propagation of numerical error from the boundary conditions. The spatial derivatives appearing in the evolution equations are approximated at every time step by finite difference methods, with order of accuracy $N_{\rm FD}$ chosen by the user. The time stepping algorithm can also be chosen from several options, but in this work we always choose the well-known 4th order Runge-Kutta method (RK4). Finally, regarding boundary conditions, NRPy+ implements the method previously described to distinguish inner and outer boundary points and to assign the corresponding values to ghost points, including the parity changes for vectors and tensors. For the outer boundaries we use a Sommerfeld radiation boundary condition, which aims to have the evolved functions act as waves that go through the boundary with minimal reflections.

B. Scalar field initial data and evolution equations

The approach used in this work to non-linearly couple a scalar field Φ to BH geometries is based on that of Okawa *et al.* [16], who developed constraint satisfying initial data for these systems. The scalar fields are described by the Klein-Gordon equation,

$$\left(\nabla^\mu \nabla_\mu - \mu_S^2\right)\Phi - V'(\Phi) = 0. \tag{23}$$

where $V'(\Phi)$ is a self-interaction potential, set to zero for the purposes of this work.

It is useful to introduce a new variable Π that will make the system first order in time, in analogy with what is done for the spatial metric γ_{ij} with the definition of the extrinsic curvature K_{ij}. This variable is defined as

$$\partial_t \Phi = -\alpha\Pi + \beta^i \partial_i \Phi, \tag{24a}$$

which acts as the evolution equation for Φ. Performing a 3+1 decomposition of eq. (23) yields the evolution equation for Π,

$$\begin{aligned}\partial_t \Pi =& \alpha\left(-e^{-4\phi}\bar{\gamma}^{ij}\partial_i\partial_j\Phi + e^{-4\phi}\bar{\gamma}^{ij}\bar{\Gamma}^k_{ij}\partial_k\Phi\right.\\ &\left.-2e^{-4\phi}\bar{\gamma}^{ij}\partial_j\Phi\partial_i\phi + K\Pi + \mu_s^2\Phi\right)\\ &- e^{-4\phi}\bar{\gamma}^{ij}\partial_j\alpha\partial_i\Phi + \beta^i\partial_i\Pi.\end{aligned} \tag{24b}$$

The minimal coupling of the scalar field evolution to the covariant BSSN equations is done through a non-zero stress-energy tensor, which plays the role of a source of gravitational field. The stress-energy tensor for a Klein-Gordon field with $V'(\Phi) = 0$ reads

$$\begin{aligned}T_{\mu\nu} =& -\frac{1}{2}g_{\mu\nu}\left(\partial_\alpha\Phi^*\partial^\alpha\Phi + \mu_S^2\Phi^*\Phi\right)\\ &+\frac{1}{2}\left(\partial_\mu\Phi^*\partial_\nu\Phi + \partial_\mu\Phi\partial_\nu\Phi^*\right).\end{aligned} \tag{25}$$

From this expression for $T_{\mu\nu}$ it is easy to derive the ADM source terms, defined in eqs. (9). These read

$$\rho = \frac{1}{2}\left(\Pi^*\Pi + \mu_S^2\Phi^*\Phi + D_k\Phi^* D^k\Phi\right), \tag{26a}$$

$$S_i = \frac{1}{2}\left(\Pi D_i\Phi^* + \Pi^* D_i\Phi\right), \tag{26b}$$

$$\begin{aligned}S_{ij} =& \frac{1}{2}\gamma_{ij}\left(\Pi^*\Pi - \mu_S^2\Phi^*\Phi - D^k\Phi^* D_k\Phi\right)\\ &+\frac{1}{2}\left(D_i\Phi^* D_j\Phi + D_i\Phi D_j\Phi^*\right).\end{aligned} \tag{26c}$$

Constraint-satisfying initial data for the Einstein-Klein-Gordon system were established by Okawa *et al.* [16] for several configurations. In this work we focus our implementation efforts on Gaussian and dipolar initial configurations for a scalar field around a Schwarzschild BH, in isotropic coordinates.

For both sets of initial data, the spacetime configuration is set up by NRPy+'s UIUC BH module, which generates initial data for a Kerr BH with mass M and dimensionless spin χ. This module is based on the work of Liu *et al.* [17], who proposed a quasi-isotropic radial coordinate r, which reduces to the Schwarzschild coordinate when $\chi = 0$, and computed the spatial metric and extrinsic curvature for the spacetime in these coordinates. These initial data allow for the stable evolution of rapidly rotating BHs. To derive the initial data for the fields, we take the ansatz

$$\Pi = \frac{\psi^{-5/2}}{\sqrt{r\pi}}F(r)\,Z(\theta,\varphi), \tag{27a}$$

$$\psi = \psi_S + \sum_{l,m}\frac{u_{lm}(r)}{r}Y_{lm}(\theta,\varphi), \tag{27b}$$

where $\psi = e^\phi$ and $\psi_S = 1 + M/2r$ is the conformal factor of the Schwarzschild metric in isotropic coordinates. Furthermore, Φ is set to zero initially. Imposing this ansatz, the momentum constraints are trivially satisfied, while the Hamiltonian constraint is reduced to an ODE for the u_{lm},

$$\sum_{lm}\left(u''_{lm} - \frac{l(l+1)}{r^2}u_{lm}\right)Y_{lm} = -F^2(r)\,Z^2(\theta,\varphi). \tag{28}$$

By setting F and Z in eq. (28) to

$$F(r) = A_{00}\sqrt{r}e^{-\frac{(r-r_0)^2}{w^2}}, \tag{29a}$$

$$Z(\theta,\varphi) = \frac{1}{\sqrt{4\pi}}, \tag{29b}$$

where r_0 and w are the Gaussian profile centre and width, respectively, we find the only non-zero u_{lm} for this configuration to be that with $l = m = 0$, which reads

$$u_{00} = A_{00}^2 \frac{w\left[w^2 - 4r_0\left(r - r_0\right)\right]}{16\sqrt{2}} \left\{ \mathrm{erf}\left[\frac{\sqrt{2}\left(r - r_0\right)}{w}\right] - 1 \right\} - A_{00}^2 \frac{r_0 w^2}{8\sqrt{\pi}} e^{\frac{-2(r-r_0)^2}{w^2}}. \tag{30}$$

This initial data configuration is spherically symmetric with a Gaussian field profile.

It is also possible to establish a dipole configuration by setting the functions F and Z to

$$F\left(r\right) = A_{11} r e^{-\frac{(r-r_0)^2}{w^2}}, \tag{31a}$$

$$Z\left(\theta, \varphi\right) = Y_{1-1} - Y_{11} = \sqrt{\frac{3}{2\pi}} \sin\theta \cos\varphi. \tag{31b}$$

The non-zero components of u_{lm} that solve eq. (28) for this choice are

$$\begin{aligned} u_{22} = u_{2-2} = &- \frac{A_{11}^2 w^2}{80 r^2} \sqrt{\frac{3}{10\pi}} e^{-\frac{2(r-r_0)^2}{w^2}} \left[4\left(r^4 + r^3 r_0 + r^2 r_0^2 + r r_0^3 + r_0^4\right) + w^2\left(4r^2 7 r r_0 + 9 r_0^2\right) + 2w^4\right] \\ &+ A_{11}^2 \sqrt{\frac{3}{5}} \frac{w\left(-16r^5 + 16 r_0^5 + 40 r_0^3 w^2 + 15 r_0 w^4\right)}{320 r^2} \left\{ \mathrm{erf}\left[\frac{\sqrt{2}\left(r - r_0\right)}{w}\right] - 1 \right\} \\ &+ A_{11}^2 \sqrt{\frac{3}{5}} \frac{w r_0\left(16 r_0^4 + 40 r_0^2 w^2 + 15 w^4\right)}{320 r^2} \left[\mathrm{erf}\left(\frac{\sqrt{2} r_0}{w}\right) + 1 \right] \\ &+ A_{11}^2 \sqrt{\frac{6}{5\pi}} e^{-\frac{2 r_0^2}{w^2}} \frac{2 w^2\left(4 r_0^4 + 9 r_0^2 w^2 + 2 w^4\right)}{320 r^2}, \end{aligned} \tag{32a}$$

$$u_{20} = -\sqrt{\frac{2}{3}} u_{22}, \tag{32b}$$

$$u_{00} = \frac{A_{11}^2 w}{16} \left\{ -\frac{2w\left(2r_0^2 + w^2\right) e^{-\frac{2(r-r_0)^2}{w^2}}}{\sqrt{\pi}} - \sqrt{2}\left[4\left(r - r_0\right) r_0^2 + \left(r - 3r_0\right) w^2\right] \left[\mathrm{erf}\left(\frac{\sqrt{2}\left(r - r_0\right)}{w} - 1\right)\right] \right\}. \tag{32c}$$

We also propose a simplified, albeit constraint-violating alternative to the pseudo-bound states detailed in [16]. The expressions for the initial data can be achieved by taking the real part of eq. (53) of the reference, and setting $Z\left(\theta\right) = \sin\theta$. The expressions for the scalar field, obtained with this method, read

$$\Phi\left(t, r, \theta, \varphi\right) = \frac{A_P}{\sqrt{\pi}} e^{\frac{-(r-r_0)^2}{w^2}} \cos\left(\omega t + m\varphi\right) \sin\theta, \tag{33}$$

$$\Pi = \frac{A_P}{\alpha\sqrt{\pi}} e^{\frac{-(r-r_0)^2}{w^2}} \left(m\beta^\varphi - \omega\right) \sin\left(\omega t + m\varphi\right) \sin\theta, \tag{34}$$

where ω is a frequency and m is an integer.

The evolution equations, BSSN source terms and initial data detailed above were implemented into NRPy+ by the construction of four modules that generate these expressions and output them to C code. To test the implementation, convergence tests were made for both the Gaussian and dipolar initial data. Since this work will be focused almost exclusively in the latter, we show in Fig. 1 we show the results for that case. For these tests, the scalar field was initialised with parameters $A_{11} = 0.075$, $r_0 = 5.0$, $w = 0.5$ and $\mu_S = 0$. The spacetime configuration was initialised with $M = 1$ and $\chi = 0$, with the boundary at $R_{\max} = 20.0$, $N_\theta = 16$ and $N_\varphi = 32$.

For this set of parameters, Fig. 1 shows a convergence of $\mathcal{H}$ to zero at the expected rate. This is especially evident in the vicinities of r_0, where the scalar field dominates, while in the rest of the domain the plots coincide if $|\mathcal{H}|$ is not rescaled, hinting at effects such as floating point precision dominating the numerical error.

V. NON-LINEAR SCATTERING OF MASSLESS SCALAR FIELDS

Now we turn our attention to the numerical simulations of massless fields in BH spacetimes performed with the implementation detailed above. For the simulations detailed in this section, the fields were initialised with the

TABLE I. Parameters for all simulations performed in this work. In the simulation names, S refers to Schwarzschild, K refers to Kerr, W means wide, N means narrow and PB means pseud-bound. For the PB case, we chose $\omega = 0.3929$ and $m = 1$.

Simulation	M	χ	A	r_0	w	μ_S	N_r	N_θ	N_φ	$R_{\max}$	w_s
SW	1	0	0.04	6.0	2.0	0	398	16	32	100.0	0.25
SN	1	0	0.075	5.0	0.5	0	544	16	32	50.0	0.37
KW	1	0.95	0.04	6.0	2.0	0	452	16	32	100.0	0.22
KN	1	0.95	0.075	5.0	0.5	0	626	16	32	50.0	0.32
PB	1	0.95	0.003	25.0	10.0	0.35	1172	8	16	1000.0	0.17

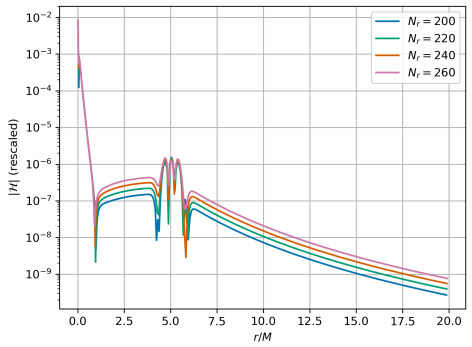

FIG. 1. Convergence tests for the nonlinear evolution of a scalar field Φ in a isotopic Schwarzschild spacetime with initial data of dipole configuration.

dipolar configuration, even in the case of rotating BHs where these initial data are constraint violating. The aim is to qualitatively explore the scattering behaviour of the fields in these spacetimes.

A. Massless scalar fields in a Schwarzschild background

To begin our qualitative study of the scalar field scattering off a Schwarzschild BH, with constraint-satisfying initial data, we performed a simulation with parameters corresponding to the SW line of Table I. To visualise the results, we performed a slicing of the spatial hypersurfaces along the plane $\varphi = \pm\pi/2$, and redefined the x coordinate accordingly. The plots for four time slices are show in Fig. 3.

The first plot to the left shows an early configuration of the field – Φ is initialised to zero, so it would be pointless to plot $t = 0$. As expected, this gives a dipolar configuration with Gaussian radial profile. The field is, then, propagated towards the origin and towards infinity. The second plot shows the begining of the interaction between the field and the event horizon, which results in the periodic emission of scalar pulses with decreasing amplitude over time. This behaviour is consistent with the quasi-normal ringdown [18], a consequence of the Teukolsky equations [19] for linear perturbations of BH spacetimes, where the perturbing fields are expected to oscillate with constant frequency ω_R with exponential damping of oscillation amplitude.

To further probe the quasi-normal oscillations of massless scalar fields in Schwarzschild geometries, a narrow field profile, corresponding to parameters SN in Table I, was evolved. Then we extracted the scalar field at the point of coordinates $r/M \approx 15$, $\theta \approx \pi/2$, $\varphi \approx 0$, as well as the gravitational wave signal, through the Weyl scalar [20] Ψ_4, decomposed into modes of $l = 2$ at $r/M \approx 30$. The results of these extractions are shown in Figs. 3 and 4. In the scalar channel, the quasi-normal ringdown is apparent: there is an exponentially damped oscillation of approximately constant frequency. At $t/M \approx 90$ we see evidence of propagation of error from the boundary, which is expected from the fact that $R_{\max}/M = 50.0$ for this simulation. The gravitational wave channel sees similar behaviour, which is consistent with the findings of Okawa *et al.* [16] and BH perturbation theory.

With the data presented above for the scalar field at a constant point, as a function of time, an attempt was made to determine the quasi-normal frequencies for the dominant modes of oscillation. This was done by decomposing the scalar signal into spherical harmonics and fitting a exponentially damped sinusoid to the data. The results of this analysis, however, were not satisfactory, revealing a 10% to 20% difference between our results and those predicted in the data files provided in [21] (see [18, 22] for details on the calculation of the quasi-normal frequencies), so we chose not to show them. The extraction of BH mass and spin shown in reference [16] for similar evolutions sheds some light on the effects that may justify this difference. The authors show that the interaction of the scalar cloud with the BH is responsible for accretion of a relevant portion of the scalar field, leading to increase of BH mass and spin-up for fields with large enough amplitude. This change of BH parameters leads to a change in the predicted quasi-normal frequencies and, in fact, the increase in BH spin of 15% to 20% shown in the reference can account for the increased quasi-normal frequency obtained from our fits. Nevertheless, without accurate measurement of BH properties, *e.g.* through the deployment of an apparent horizon finder, we can not take this argument with certainty.

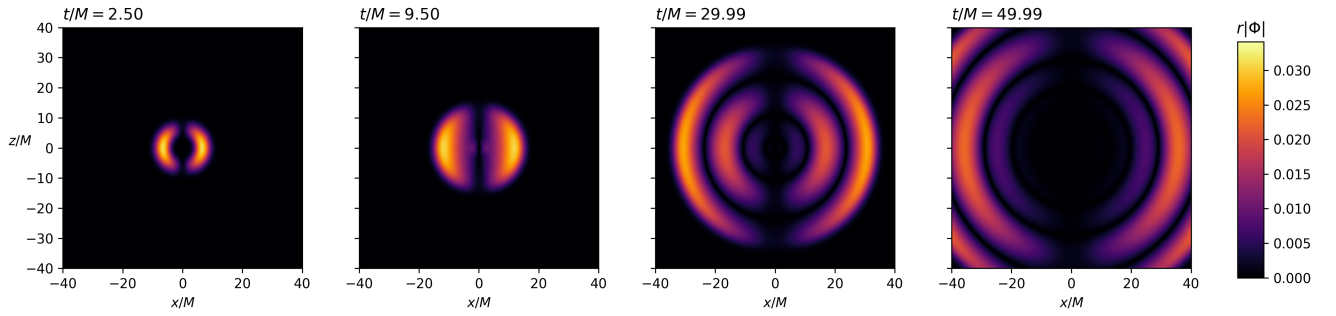

FIG. 2. Snapshots of the scalar field profile in a Schwarzschild background, for four instants of time, corresponding to parameters SW of Table I.

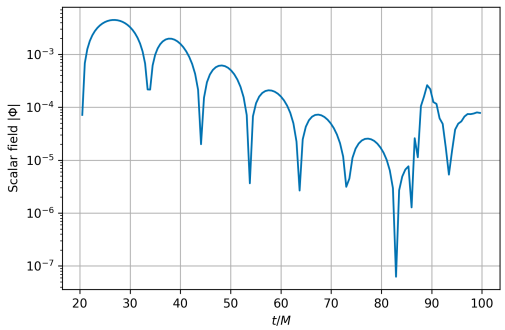

FIG. 3. Quasi-normal ringdown of a Schwarzschild BH, seen in the scalar channel.

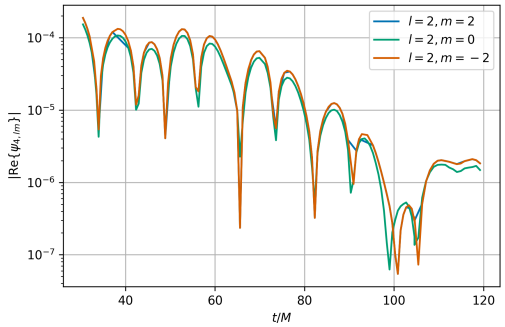

FIG. 4. Quasi-normal ringdown of a Schwarzschild BH, seen in the gravitational wave channel.

B. Massless scalar fields in a Kerr background

To gain a phenomenological understanding of how the scattering situation, studied above, would change if it occurred in a rotating BH background, and even though the initial data implemented for the scalar field violate the constraints for these spacetimes, two simulations were performed, in analogy with the non-spinning case. For the first simulation, corresponding to the parameters KW of Table I, we proceeded in a similar way to the Schwarzschild case and ploted the scalar field profile on a plane of $\varphi = \pm\pi/2$ for four coordinate time values. These are shown in Fig. 5. Comparison with the Schwarzschild case of Fig. 2 shows an asymmetry of the scalar profile, which wasn't present in the previous case. This might be explained by the frame dragging effects present in the Kerr geometry, which force the field to co-rotate with the BH near the horizon. Nevertheless, evidence of quasi-normal oscillation is still present, as before.

Following, again, the same path as for the Schwarzschild case, a narrower field profile was evolved in order to better probe the quasi-normal oscillations in the Kerr geometry. The initial data parameters for this simulation are listed in Table I, corresponding to the KN case. To obtain a visualisation of the quasi-normal ringdown, we again sampled the scalar field at $r/M \approx 15$, $\theta \approx \pi/2$, $\varphi \approx 0$, and plotted the results in Fig. 6 as a function of coordinate time t. Comparing with the results of Fig. 3, we observe that the spinning case is characterised, at least on average, by a greater oscillation frequency – we see around 8 half-periods of oscillation in this case before the boundary effects dominate, compared to around 6 in the Schwarzschild case. This observation is consistent with perturbative calculations of the frequencies of quasi-normal modes for Kerr BHs, as ω_R, the real part of the quasi-normal frequency $\omega_{\rm QNM}$ should increase when the dimensionless spin χ increases for the dominant $l, m = 1, \pm 1$ modes. However, both the oscillation frequency and the exponential damping parameter appear not to be constant over time. This can be due to the aforementioned change of BH parameters from accretion and superradiant amplification of the field, but also from the fact that rapidly spinning BHs are capable of exciting modes with larger l, which decay faster than the fundamental modes, leading to a mixture of modes at early times.

In Fig. 7 we show the decomposition of the gravitational wave signal into $l = 2$ spin-weighted spherical harmonics at $r/M \approx 30$ for simulation KN. Comparing with the results for simulation SN show a split between the $m = 0$ mode and the $m = \pm 2$ modes, which wasn't present in the previous case. However, as before, the

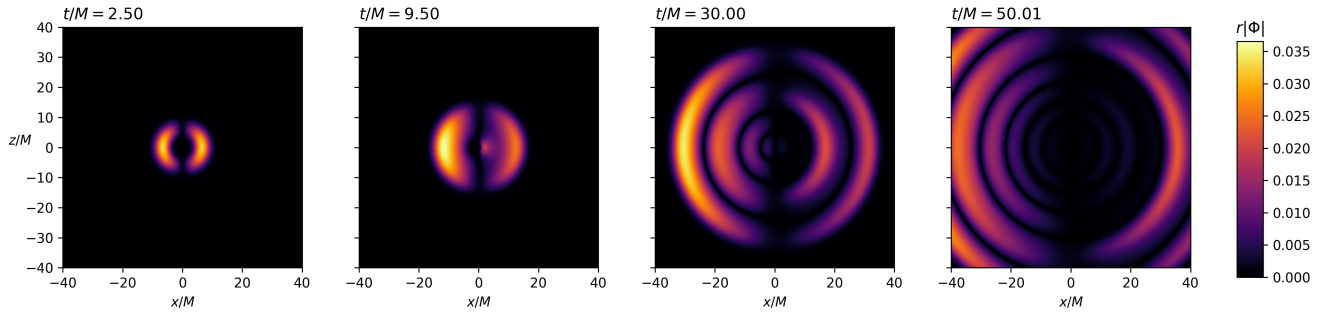

FIG. 5. Snapshots of the scalar field profile in a Kerr background, for four instants of time, corresponding to parameters KW of Table I.

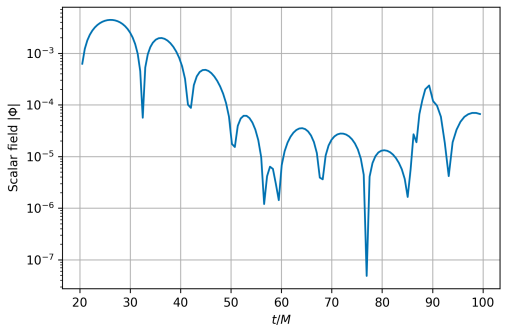

FIG. 6. Quasi-normal ringdown of a Kerr BH, seen in the scalar channel.

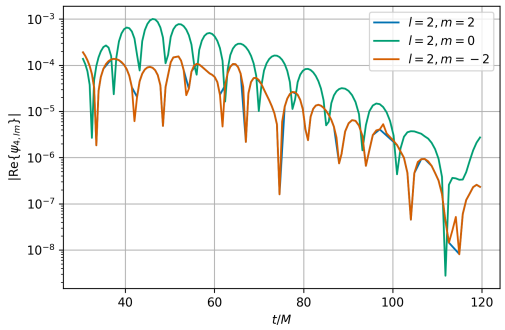

FIG. 7. Quasi-normal ringdown of a Kerr BH, seen in the gravitational wave channel.

behaviour is consistent with the expected quasi-normal ringdown, where the metric oscillates with a definite frequency and approximately exponential decay in amplitude over time.

VI. PSEUDO-BOUND STATES OF MASSIVE SCALAR FIELDS

To conclude our analysis, we now show the results for the evolution of a pseudo-bound initial state around a Kerr BH, corresponding to parameters PB in Table I. These can be seen in Fig. 8. Contrary to the previous plots of this kind, here we show an equatorial slicing of the spatial hypersurfaces. The plot on the left shows the initial configuration of Φ, which evolves by being propagated in both radial directions. Furthermore, in the second plot, the scalar cloud is observed to be rotating, which is consistent both with the initial data imposed as well as the frame-dragging effects of the Kerr geometry. The two middle plots show the emission and propagation of quasi-normal modes, but these propagate slower than in the massless cases above due to the attractive potential created by the non-zero mass coupling μ_S. Finally, the two plots on the right show the creation of a long-lived scalar cloud which slowly disperse over time. These results are consistent with those for constraint-satisfying pseudo-bound states presented by Okawa *et al.* [16].

For this simulation the Weyl scalar Ψ_4 was also extracted, at $r/M \approx 30$, and decomposed into spin-weighted spherical harmonics. Other than the expected quasi-normal ringdown shown in all previous simulations, there were no distinguishing features of the pseudo-bound modes in the gravitational wave channel, which we attribute to the short evolution performed (the time scales for superradiant instabilities are much larger than our evolution time). Therefore, for the sake of brevity, we omit a graphical display of these results here, leaving it to the main document of this thesis.

VII. CONCLUSIONS

The analysis of the previous sections shows that this work has achieved a successful implementation of the evolution equations and initial data for a Klein-Gordon field into NRPy+. This was shown by the observation of quasi-normal modes in both scalar and gravitational wave channels, as well as the creation of long-lived scalar clouds from pseudo-bound initial data. However, the work is not without its shortcomings, the most prominent of which being the lack of precise measurement of significant quantities, such as quasi-normal frequencies

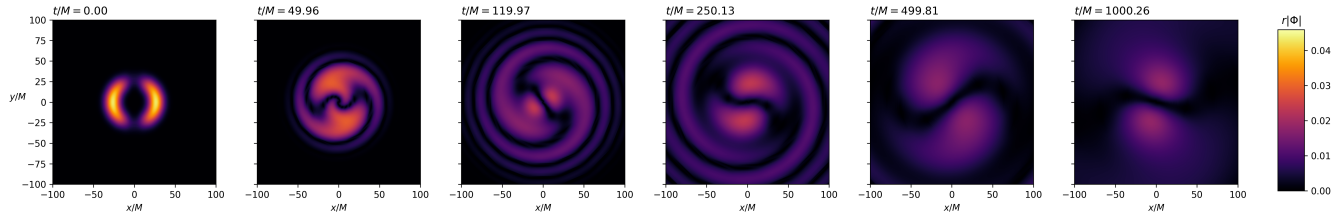

FIG. 8. Snapshots of the scalar field profile, initialised to a pseudo-bound state in a Kerr background, corresponding to parameters PB of Tab. I.

and time evolution of BH mass and spin.

Most of the shortcomings can be justified by the time constraints this type of work is subject to. Indeed, implementation of features into an already complex NR code is not trivial, and many challenges had to be faced along the way. Therefore, this work should be regarded as an early implementation, to be completed by future works. Amongst the many features that should be added to the implementation, we highlight constraint-satisfying initial data for scalar fields in Kerr geometries, constraint-satisfying pseudo-bound states and the ability to evolve complex fields as the main priorities of future efforts. Such implementations would allow for the exploration of yet uncharted effects, such as the superradiant instability for scalar fields, which would, in turn, be useful for dark matter searches and experiments probing beyond Standard Model physics in astrophysical scenarios.

[1] F. W. Dyson, A. S. Eddington, and C. Davidson, IX. A determination of the deflection of light by the sun's gravitational field, from observations made at the total eclipse of May 29, 1919, Phil. Trans. R. Soc. A **220**, 291 (1920).

[2] B. P. A. *et al.* (LIGO Scientific Collaboration & Virgo Collaboration), Observation of gravitational waves from a binary black hole merger, Phys. Rev. Lett. **116**, 061102 (2016).

[3] E. T. Newman, E. Couch, K. Chinnapared, A. Exton, A. Prakash, and R. Torrence, Metric of a rotating, charged mass, J. Math. Phys. **6**, 918 (1965).

[4] R. Brito, V. Cardoso, and P. Pani, *Superradiance*, 2nd ed., Lecture Notes in Physics, Vol. 971 (Springer International Publishing, 2020).

[5] Y. B. Zel'dovich, Amplification of cylindrical electromagnetic waves reflected from a rotating body, Zh. Eksp. Tear. Fiz. **62**, 2076 (1972).

[6] R. Arnowitt, S. Deser, and C. W. Misner, Republication of: The dynamics of general relativity, Gen Relativ Gravitn **40**, 1997 (2008).

[7] E. Gourgoulhon, *3+1 Formalism in General Relativity: Bases of Numerical Relativity*, 1st ed., Lecture Notes in Physics, Vol. 846 (Springer-Verlag Berlin Heidelberg, 2012).

[8] M. Alcubierre, *Introduction to 3+1 numerical relativity* (Oxford University Press, 2008).

[9] T. W. Baumgarte and S. L. Shapiro, *Numerical Relativity: Solving Einstein's Equations on the Computer* (Cambridge University Press, 2010).

[10] M. Shibata and T. Nakamura, Evolution of three-dimensional gravitational waves: Harmonic slicing case, Phys. Rev. D **52**, 5428 (1995).

[11] T. W. Baumgarte and S. L. Shapiro, Numerical integration of Einstein's field equations, Phys. Rev. D **59**, 024007 (1998).

[12] J. D. Brown, Covariant formulations of Baumgarte, Shapiro, Shibata, and Nakamura and the standard gauge, Phys. Rev. D **79**, 104029 (2009).

[13] M. Alcubierre, B. Brügmann, P. Diener, M. Koppitz, D. Pollney, E. Seidel, and R. Takahashi, Gauge conditions for long-term numerical black hole evolutions without excision, Phys. Rev. D **67**, 084023 (2003).

[14] I. Ruchlin, Z. B. Etienne, and T. W. Baumgarte, SENR/NRPy+: Numerical relativity in singular curvilinear coordinate systems, Phys. Rev. D **97**, 064036 (2018).

[15] L. Dagum and R. Menon, Openmp: an industry standard api for shared-memory programming, IEEE Comput. Sci. Eng **5**, 46 (1998).

[16] H. Okawa, H. Witek, and V. Cardoso, Black holes and fundamental fields in numerical relativity: Initial data construction and evolution of bound states, Phys. Rev. D **89**, 104032 (2014).

[17] Y. T. Liu, Z. B. Etienne, and S. L. Shapiro, Evolution of near-extremal-spin black holes using the moving puncture technique, Phys. Rev. D **80**, 121503 (2009).

[18] E. Berti, V. Cardoso, and A. O. Starinets, Quasinormal modes of black holes and black branes, Class. Quantum Gravity **26**, 163001 (2009).

[19] S. A. Teukolsky, Perturbations of a Rotating Black Hole. I. Fundamental Equations for Gravitational, Electromagnetic, and Neutrino-Field Perturbations, Astrophys. J. **185**, 635 (1973).

[20] E. Newman and R. Penrose, An approach to gravitational radiation by a method of spin coefficients, J. Math. Phys. **3**, 566 (1962).

[21] V. Cardoso, Ringdown data and routines, (accessed: 21/12/2020).

[22] E. Berti, V. Cardoso, and C. M. Will, Gravitational-wave spectroscopy of massive black holes with the space interferometer LISA, Phys. Rev. D **73**, 064030 (2006).